© S. Hirzel Verlag
Stuttgart
ACUSTICA
Vol. 80 (1994)

On the Stability of Bowed String Motion

J. Woodhouse
Cambridge University Engineering Department, Cambridge, UK

On the Stability of Bowed String Motion

Summary

Linearised stability analysis is carried out for periodic solutions to a range of idealised theoretical models of the motion of a bowed string. For the simplest case, it is possible to obtain a quantitative value for the stability threshold by an approach based on space-time diagrams, which has considerable physical and intuitive appeal. For the more general cases it is necessary to resort to computation, and two different state-vector formulations are given, each of which sheds light on aspects of the behaviour in certain models. The final formulation allows stability analysis to be carried through for the most general class of rounded-corner models. Representative results are given for the various aspects of each model, and their physical interpretation discussed.

Über die Stabilität der Bewegung einer gestrichenen Saite

Zusammenfassung

Es wird eine linearisierte Stabilitätsuntersuchung für periodische Lösungen verschiedener idealisierter theoretischer Modelle der Bewegung einer gestrichenen Saite ausgeführt. Im einfachsten Fall kann man einen quantitativen Wert für die Stabilitätsgrenze auf der Grundlage von Raum-Zeit-Diagrammen erhalten, was von beträchtlichen physikalischem und intuitivem Reiz ist. Für allgemeinere Fälle muß man Zuflucht zu Berechnungen suchen, und es werden zwei verschiedene Formulierungen mit Zustandsvektoren angegeben, von denen jede verschiedene Aspekte des Verhaltens in gewissen Modellen beleuchtet. Die endgültige Formulierung erlaubt die Durchführung einer Stabilitätsuntersuchung für die allgemeinste Klasse von Modellen der „abgerundeten Ecken". Es werden repräsentative Ergebnisse für die verschiedenen Aspekte jedes Modells angegeben und ihre physikalische Interpretation wird diskutiert.

Sur la stabilité du mouvement d'une corde frottée

Sommaire

On procède à une analyse de la stabilité des solutions périodiques déduites de divers modèles théoriques du mouvement d'une corde frottée. Dans le cas le plus simple il est possible d'obtenir une estimation quantitative du seuil de stabilité, à partir d'une analyse basée sur des diagrammes espace-temps qui est très attrayante du double point de vue physique et intuitif. Pour les cas plus généraux, on ne peut éviter le recours au calcul; et nous présentons deux formulations differentes de vecteur d'état, chacune apportant quelque éclaircissement sur le comportement de certains modèles. La formulation finale permet de mener à bien l'analyse de la stabilité pour la catégorie la plus générale des modèles à angles arrondis. On fournit des résulats représentatifs des divers aspects de chaque modèle, et on discute leur interprétation physique.

1. Introduction

Studies of the motion of a bowed string can be divided into two broad categories. First, periodic motion produced by steady bowing can be investigated by a variety of means, analytical, computational and heuristic. Such studies have revealed a very rich set of possible periodic regimes, including the "Helmholtz motion" which is the one generally sought by players of bowed-string instruments [1–3]. For such regimes, the allowed ranges of the various parameters controlled by the player (bow force, bow speed and bow position on the string) can be found, by approximate analytical calculations [4–7] or by numerical simulation [7–9]. For a given oscillation regime, the variation of detailed motion within those allowed ranges can be similarly investigated. Particularly for the Helmholtz motion, several such studies have been made [5, 10]. These have shed light on many aspects of the behaviour of real bowed strings.

However, many practical problems related to bowed strings cannot be investigated in this way, since they involve transient behaviour of one kind or another. This second category of study is far harder, and far less progress has been made at the present time. As a result of the strong nonlinearity arising from stick-slip friction, which drives all bowed-string motion, transients can in general only be investigated seriously via numerical simulation [7]. The only exception, which to an extent bridges the gap between the two categories of study, is the investigation of the stability of periodic

Received 5 November 1992,
accepted 7 January 1993.

J. Woodhouse, Cambridge University Engineering Department, Trumpington Street, Cambridge CB2 1PZ, U.K.

oscillation regimes. By assuming a small perturbation superimposed on a periodic motion, one may be able to establish whether this perturbation tends to grow or decay with time. A requirement of stability may put further constraints on the allowed ranges of the player's parameters, so that it adds information to the periodic-motion studies. At the threshold of instability the analysis may predict a particular form of perturbation to be the first to go unstable, and this gives a clue, at least, as to how the motion will subsequently evolve. The analysis may soon break down, being based on an assumption of a small perturbation to a given periodic regime, but one can at least make a guess as to which other periodic regime will eventually take over as the perturbation becomes large.

To perform a stability analysis, a particular theoretical model is required. It is easiest to make quantitative progress using the very simple model due to Raman [1], the scope and limitations of which have been discussed elsewhere [2]. In this study, Raman's model will be used to establish methods and to discover the physical mechanism and nature of possible instabilities. The method of analysis is based initially on space-time diagrams. This approach, introduced in an earlier paper [11], has the advantage of making explicit an aspect of the physics of instability which is not heavily dependent on a particular theoretical model. After detailed results have been obtained from Raman's model, the analysis method is extended to the case of rounded-corner models [6, 7].

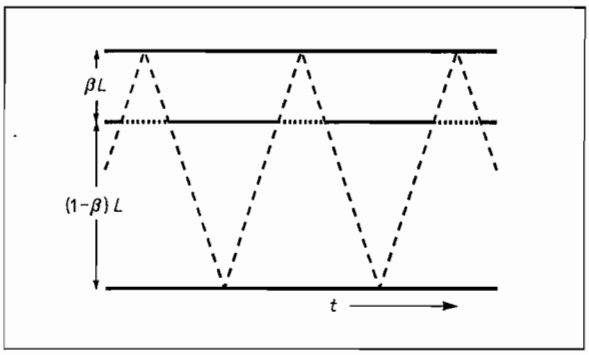

Fig. 1. Space-time diagram, showing the path of the Helmholtz corner (dashed line). Time is plotted horizontally, distance along the string vertically. The position of the bow is marked by a horizontal line, plotted solid where the bow and string are sticking and dotted where they are slipping.

2. Stability of solutions to the Raman model

2.1. Subharmonics

The Helmholtz motion is characterised by a single "corner", or velocity discontinuity, reflecting back and forth between the ends of the string. In a space-time diagram, it follows the path shown dashed in Fig. 1. The slope of the line segments is governed by the wave speed on the string. Now suppose that the bow is applied a distance βL from one end of the string, L being the total length of the string. At that point, appearing as a horizontal line in the space-time diagram, the contact conditions alternate between states of sticking friction and sliding friction, transitions being triggered by the passage of the Helmholtz corner. This alternation is indicated in Fig. 1 by showing a solid line where the bow and string are sticking, and a dotted line where there is slipping.

If we now introduce a small, spatially-localised perturbation to the ideal Helmholtz motion, it will travel along a trajectory parallel to that of the Helmholtz corner while it is on the free string. The difference comes when it impinges on the bow, and what happens then depends upon whether the bow-string contact is sticking or sliding at that moment. Once a model has been constructed for the interaction with a sticking and a sliding bow, it is possible to follow the trajectory of the perturbation in the space-time diagram, with due regard for any interactions with perturbations initiated on other trajectories, and thus predict whether a general perturbation can grow with time or whether all possible perturbations will decay.

The detailed behaviour found in such an analysis depends on the model employed to describe the string motion and the frictional force. The simplest possible model for the string allows transverse motion only, described by the familiar wave equation. Interaction with the bow is very easily described within this model. If torsional motion of the string is included, things are more complicated since an incident transverse wave scatters some of its energy into torsional waves during any interaction with friction at the bow. These will follow different trajectories in the space-time diagram since the torsional wave speed is different from the transverse wave speed (usually faster), and they may later scatter back into transverse motion by further interactions at the bow (or perhaps at the terminations of the string). Further complications, which are probably less important but which certainly influence the detailed motion, come from bending stiffness in the string [4–6], and the finite width of the ribbon of bow-hair in contact with the string [11].

Similar remarks can be made about models of the frictional force: the simplest model gives a very straightforward answer, but it is inadequate to describe the tribological behaviour of rosined surfaces fully, with consequences which have yet to be properly explored. This simplest model, the "friction-curve model", is the familiar one which assumes that the

friction force depends only on the instantaneous relative velocity of the bow and the surface of the string, according to a relation like that sketched in Fig. 2. The vertical portion of the curve describes the indeterminacy of friction force during sticking, provided the limit of sticking friction is not exceeded. The curved portions describe sliding.

First, we examine the behaviour of a perturbation to the Helmholtz motion as it interacts with a sticking and a sliding bow, using the simplest models for both string and friction force. The sticking bow is particularly simple in this case; since the string velocity is fixed at the bow speed v_b, any velocity perturbation incident on the sticking bow must be perfectly reflected with a reflection coefficient of -1. There is no transmitted wave. This simple interaction is shown schematically in Fig. 3 a.

The sliding bow requires a little more calculation. The sliding speed of the Helmholtz motion, $v_s = -v_b(1/\beta - 1)$, determines an "operating point" on the friction curve. A small perturbation will only be influenced by the friction curve behaviour near this point, so we may linearise the friction-velocity relation:

$$f(v_s + \delta v) \approx f(v_s) + \delta v\, f'(v_s) = f_b(c + k\,\delta v), \quad (1)$$

say, for the velocity perturbation δv. The normal force between bow and string, f_b, appears as a scalar multiplier on the friction-velocity relation. It is explicitly included for notational consistency with ref. [2]. The constant force $c f_b$ is associated with the ideal Helmholtz motion. It causes a constant, static slope discontinuity in the string at the bowed point. Since it plays no role in the dynamics, it may be ignored in the perturbation analysis. Now carrying out a standard calculation of the reflection and transmission coefficients r and t at the bowed point, when the linearised force-velocity relation is imposed on an ideal string of tension T and line density m, we obtain

$$t = \frac{2}{2 - k f_b Y_0} = 1 + \zeta, \quad (2)$$

say, where

$$\zeta = \frac{k f_b Y_0}{2 - k f_b Y_0} \approx \frac{k f_b Y_0}{2}, \quad (3)$$

and where $Y_0 = (T m)^{-1/2}$ is the wave admittance of the string. Correspondingly,

$$r = \zeta \approx \frac{k f_b Y_0}{2}. \quad (4)$$

These results are illustrated schematically in Fig. 3 b. The approximate results exploit the fact that $k f_b Y_0$ is generally small. If k is positive, as is expected for sliding friction, the transmitted signal is slightly amplified by interaction with the bow, an effect commonly described as "negative resistance" [12]. This amplification is the source of any possible instability (at least within this linearised analysis): all other influences on a perturbation are dissipative, and the stability threshold is determined by the condition that the total effect of dissipative phenomena just balances that of amplification at the sliding bow.

If scattering of transverse waves into torsional waves at the bow is allowed, the interaction of a perturbation with the bow is somewhat more complicated. Only the simplest model of this process will be treated. If any reflection of torsional waves from the

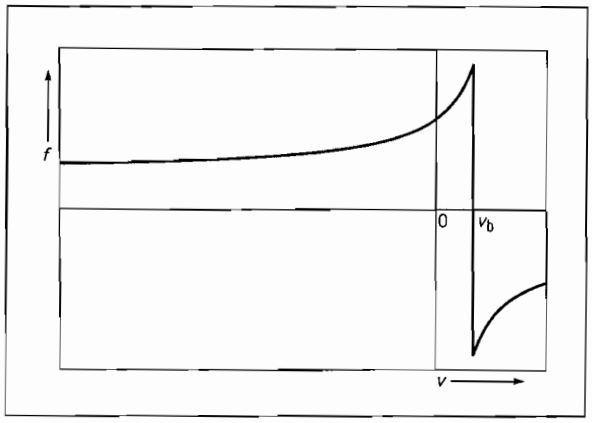

Fig. 2. Typical relation between frictional force f and string velocity v at the bowed point.

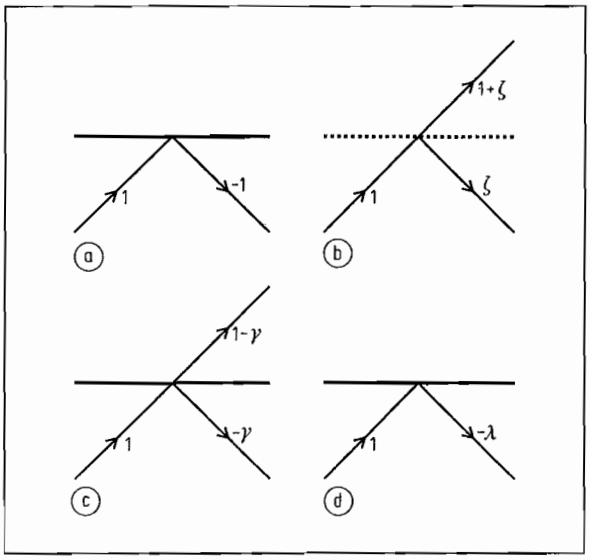

Fig. 3. Interactions of a localised velocity perturbation with the bow and the string's terminations: a) interaction with a sticking bow without torsional coupling; b) interaction with a slipping bow; c) interaction with a sticking bow with coupling to torsional waves; d) interaction with one boundary of the string, within Raman's model.

string terminations is neglected, so that torsional waves are simply ignored once they have been generated, then they may be allowed for by a simple transformation of the friction-velocity relation involving a linear shear [8]. For interaction with the sliding bow, the result is merely a change in the value of ζ, and requires no further analysis. Interaction with the sticking bow, on the other hand, is made significantly more complicated. The sticking portion of the $f(v)$ relation is no longer vertical, but becomes a straight line with a finite negative slope $-A f_b$, say (determined by the impedance ratio between torsional and transverse waves). The analysis of eqs. (1)–(4) may be applied, so that the transmission and reflection coefficients are

$$t = \frac{2}{2 + A f_b Y_0} = 1 - \gamma, \tag{5}$$

say, where

$$\gamma = \frac{A f_b Y_0}{2 + A f_b Y_0}, \tag{6}$$

and

$$r = -\gamma. \tag{7}$$

If coupling to torsion is weak, γ will be close to unity so that the transmitted wave is small. As expected, the interaction (so far as transverse waves are concerned) is dissipative. It is shown schematically in Fig. 3c.

Neglecting for the moment the reflected waves generated at the slipping bow, and without any scattering into torsional waves, the path of a perturbation may be readily plotted in the space-time diagram. Two examples are shown in Fig. 4. As has been pointed out before [11], any such path is periodic with a period which makes it a subharmonic of the Helmholtz motion. It will be referred to as an "elemental subharmonic path". The order of the subharmonic depends on the bow position β. When $\beta = 1/n$, all possible elemental paths correspond to an nth subharmonic. For general β, elemental paths are possible with subharmonic periods given by the two nearest integers to $1/\beta$, the choice depending on the phase with respect to the Helmholtz motion. This is illustrated in Fig. 4: the two cases show the same value of $\beta = 0.3$, and a difference of phase produces a third subharmonic in case (a), while case (b) gives a fourth subharmonic. Subharmonic activity echoing the behaviour of these elemental paths certainly occurs in some form on real violin strings, since it is occasionally audible. A description of how best to elicit audible subharmonics is given in ref. [11].

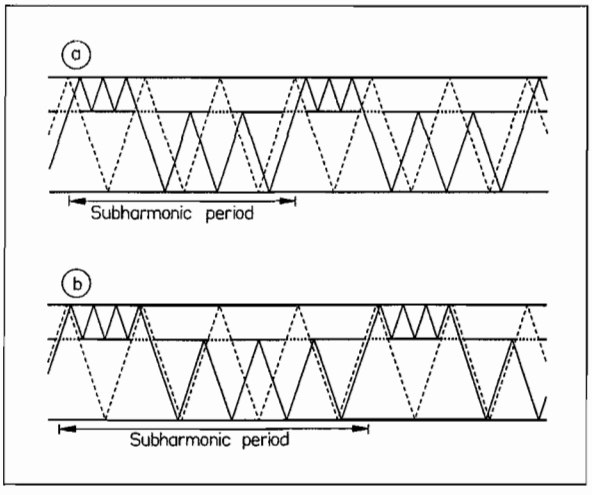

Fig. 4. Subharmonic paths in the space-time diagram. For $\beta = 0.3$, elemental subharmonic paths are possible with subharmonic order a) 3 and b) 4, depending on the phase with respect to the Helmholtz motion.

2.2. Stability for $\beta = 1/n$ without torsional interaction

To obtain a quantitative stability threshold it is first necessary to complete the specification of the model. If no energy dissipation is included in the model, it is plain that nothing will counteract the amplification effect just described, and all perturbations will be unstable (or at best neutrally stable). This general instability was first noted by Friedlander [13]. Dissipation on a real string occurs during wave propagation along the string and in the reflection processes from the string's terminations (and also from losses into torsional waves, discussed above). In practice propagation and reflection effects are accompanied by wave dispersion, which complicates the analysis considerably.

To obtain quantitative results which capture at least some of the essential physics, we use the only model which does not have this complication, Raman's model. The string is assumed to be an ideal, lossless, nondispersive textbook string. Dissipation occurs only at the terminations, where a simple reflection coefficient is assumed (independent of frequency). For simplicity, the same reflection coefficient will be assumed at both ends of the string. It will be denoted $-\lambda = -(1 - \varepsilon)$, where ε will generally be small. (The negative sign is included because any remotely realistic string termination is approximately a fixed point, which produces an inverted reflection.) This boundary reflection is shown schematically in Fig. 3d.

Now that the interaction of a localised velocity perturbation with the sticking bow, the sliding bow, and the string's terminations are all known, it is possible to calculate a stability threshold for the assumed Helmholtz motion. For the special case in which $\beta = 1/n$, without torsional interactions, this can be done approximately in closed form. It is necessary to take

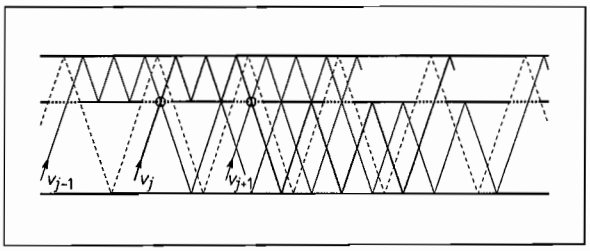

Fig. 5. For $\beta = 1/3$ and without allowance for torsional coupling, a typical elemental subharmonic path, shown as a heavy line, interacts with only two other elemental paths, shown as lighter lines. The interactions occur at the ringed points, at the slipping bow.

account of the reflections produced at the sliding bow (according to eq. (3)). These couple together elemental subharmonic paths which pass through different "windows" of sliding during the subharmonic period, as is illustrated in Fig. 5. The heavier curve shows a portion of one particular elemental subharmonic path, for $\beta = 1/3$. In the course of one subharmonic period it interacts with the two elemental paths shown as lighter curves. Interactions occur at the ringed points, by the mechanism sketched in Fig. 3 b.

It is thus necessary to find the pattern of amplitudes on the n different elemental paths which is least stable. Let the amplitude of perturbation passing upwards through the jth "window" be v_j. This interacts with any other elemental path which crosses it at the slipping bow. We seek eigenvector solutions, such that

$$v_{j+n} = \Omega v_j \tag{8}$$

where Ω is the growth (or decay) factor per subharmonic period. Since a given elemental path meets the slipping bow twice per subharmonic period, within that time it interacts with just two other paths, which are the ones corresponding to amplitudes v_{j-1} and v_{j+1}, as may be seen from Fig. 5. Following the paths through one subharmonic period, the amplitude evolution may thus be seen to be governed by

$$\Omega v_j = \lambda^{2n}(1+\zeta)^2 v_j - \zeta(1+\zeta)^2\lambda^{3n} v_{j-1} - \zeta(1+\zeta)\lambda^n v_{j+1}. \tag{9}$$

Linearising the right-hand side, treating ζ and ε as small quantities,

$$\Omega v_j \approx (1 - 2n\varepsilon + 2\zeta) v_j - \zeta v_{j-1} - \zeta v_{j+1}. \tag{10}$$

This has the form of a matrix eigenvalue problem, which is readily solved by noting that the eigenvectors take the form

$$v_j = v_0 \, e^{2\pi i j r/n} \tag{11}$$

where v_0 is a constant, and r is an integer between 0 and $n-1$. Substituting into eq. (10), the growth rates Ω are found to be

$$\Omega_r \approx 1 - 2n\varepsilon + 2\zeta(1 - \cos 2\pi r/n). \tag{12}$$

This clearly shows the competition between amplification (from the term containing ζ) and dissipation (from the term containing ε). The value of growth rate based purely on the elemental subharmonic path of Fig. 4 a would be given by eq. (12) without the cosine term. That term represents the modification arising from the interaction of elemental paths.

The threshold for stability may now be calculated from the fastest of these growth rates. If n is even, this clearly arises when $r = n/2$, while if n is odd it arises when $r = (n-1)/2$. The threshold depends only on the ratio of ε to ζ, which we denote α (following ref. [2], eq. (16) et seq.):

$$\alpha = \frac{\zeta}{\varepsilon} = \begin{cases} n/2 & (n \text{ even}) \\ n/[1 - \cos\pi(n-1)/n] & (n \text{ odd}) \end{cases}. \tag{13}$$

For values of α in excess of these the Helmholtz motion is unstable, while for values less than these it is stable. The pattern corresponding to the fastest growth rate follows from substituting the critical value of r into eq. (11). When n is even the stability threshold always corresponds to an eigenvector $[-1, 1, -1, 1, -1 \ldots]$, so that the pattern is in fact an octave subharmonic, regardless of the value of n. When n is odd, the threshold pattern is always an nth subharmonic, but as n becomes large it can be described as a slowly-modulated octave subharmonic.

The possibility, seen for the first time in this example, of elemental subharmonics combining to give eigenvectors with a shorter periodicity will be met repeatedly. Any period which is a factor of the period of the elemental path may occur. An extreme case, which has been highlighted by Weinreich and Caussé [14], occurs when the amplitudes on the elemental paths combine in such a symmetric way that the total pattern has the same periodicity as the underlying periodic motion whose stability is being investigated. We might call these "unsubharmonics". Such a solution occurs in the example just analysed, for $r = 0$. The eigenvector from eq. (11) is then simply $[1, 1, 1, \ldots, 1]$. For this case, the corresponding "growth" rate is the least unstable of all the possible values. It receives no amplification from the slipping bow but still experiences dissipation from the string's terminations, so that it does not grow under any circumstances. It will emerge later that this behaviour is characteristic of the case $\beta = 1/n$, but that for more general β such "unsubharmonics" frequently provide the most unstable perturbation pattern, which governs the stability threshold. The physical reason for this behaviour will be discussed in section 2.5.

2.3. A computational approach for the general case

For more general values of β, or when torsional interactions at the bow are included, or for periodic solutions more complicated than the Helmholtz motion, stability analysis is more difficult. For general β, elemental subharmonic paths exist with two different periodicities, which interact with each other. To follow these interactions, even in the absence of torsional coupling, is quite complicated. With torsional coupling, elemental subharmonic paths couple together at every time step, not only when the bow-string contact is slipping. Again, this makes it hard to write down an equivalent of eq. (9). Finally, for periodic solutions other than the Helmholtz motion the "building blocks" of the perturbation analysis are more complicated than the elemental subharmonic paths such as shown in Fig. 4.

All these factors make it laborious to use the approach of the previous section, or indeed to pursue closed-form analytical arguments by any approach. However, an alternative methodology can be developed, again inspired by the space-time diagram, which allows stability thresholds to be computed for the most general case of periodic solutions to the Raman model. The physical insights from the space-time diagram, and the calculation of the previous section, can be used to offset some of the shortcomings of a purely computational approach (compared with a closed-form solution).

At a given time instant, the state of a perturbation to any specified periodic solution may be characterised by a vector of amplitudes. The approach is then to construct a matrix which transforms this state vector into the corresponding state vector after one period of the underlying periodic motion. The eigenvectors and eigenvalues of this transfer matrix allow a judgement to be made about stability, and also give information about the associated physical behaviour. The matrix is constructed from a product of matrices, each of which describes the transformation of the state vector in a single time step.

It is easiest to develop the method through a specific example, so consider the case $p = 2$, $q = 3$. The length of the string is subdivided into five equal segments, and within the Raman model it is only necessary to consider perturbations which have constant velocity within each segment [2, 13]. The state of a general perturbation in the nth time step may thus conveniently be described by a 10-element vector $[u_1^{(n)}, d_1^{(n)}, u_2^{(n)}, d_2^{(n)}, \ldots, u_5^{(n)}, d_5^{(n)}]^t$, denoting amplitudes on paths passing up and down through these five segments, as illustrated in Fig. 6. It is straightforward to represent the transformation of this vector after one time step, based on the interactions shown in Fig. 3.

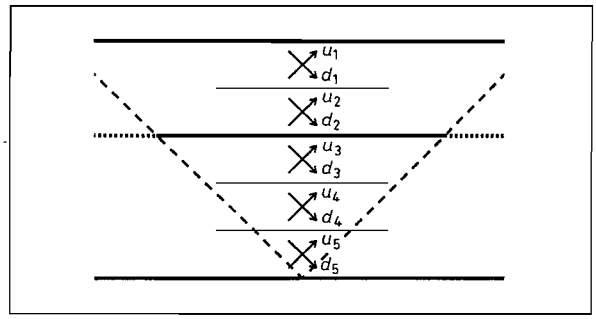

Fig. 6. For the case $p = 2$, $q = 3$ the state of a perturbation to the Helmholtz motion, or to any other periodic solution, within Raman's model may be fully characterised by amplitudes of waves passing in the two directions through each of the five subdivisions of the string's length. These amplitudes are labelled $[u_1^{(n)}, d_1^{(n)}, u_2^{(n)}, d_2^{(n)}, \ldots, u_5^{(n)}, d_5^{(n)}]^t$ to form the state vector for the stability analysis described in the text.

Two different transformation matrices are needed, depending on whether the underlying Helmholtz motion is sticking or slipping at the bow in this particular time interval. During slipping, the result is:

$$\begin{bmatrix} u_1^{(n+1)} \\ d_1^{(n+1)} \\ u_2^{(n+1)} \\ d_2^{(n+1)} \\ u_3^{(n+1)} \\ d_3^{(n+1)} \\ u_4^{(n+1)} \\ d_4^{(n+1)} \\ u_5^{(n+1)} \\ d_5^{(n+1)} \end{bmatrix} = \begin{bmatrix} 0 & 0 & 1 & 0 & 0 & 0 & 0 & 0 & 0 & 0 \\ -\lambda & 0 & 0 & 0 & 0 & 0 & 0 & 0 & 0 & 0 \\ 0 & 0 & 0 & \zeta & 1+\zeta & 0 & 0 & 0 & 0 & 0 \\ 0 & 1 & 0 & 0 & 0 & 0 & 0 & 0 & 0 & 0 \\ 0 & 0 & 0 & 0 & 0 & 0 & 1 & 0 & 0 & 0 \\ 0 & 0 & 0 & 1+\zeta & \zeta & 0 & 0 & 0 & 0 & 0 \\ 0 & 0 & 0 & 0 & 0 & 0 & 0 & 0 & 1 & 0 \\ 0 & 0 & 0 & 0 & 0 & 1 & 0 & 0 & 0 & 0 \\ 0 & 0 & 0 & 0 & 0 & 0 & 0 & 0 & 0 & -\lambda \\ 0 & 0 & 0 & 0 & 0 & 0 & 0 & 1 & 0 & 0 \end{bmatrix} \begin{bmatrix} u_1^{(n)} \\ d_1^{(n)} \\ u_2^{(n)} \\ d_2^{(n)} \\ u_3^{(n)} \\ d_3^{(n)} \\ u_4^{(n)} \\ d_4^{(n)} \\ u_5^{(n)} \\ d_5^{(n)} \end{bmatrix} \tag{14}$$

while during sticking (with torsional interaction), the matrix differs in that ζ must be replaced everywhere by $-\gamma$. (Without torsional interaction, $\gamma = 1$.) Denote these two transformation matrices $\boldsymbol{M}_1$ and $\boldsymbol{M}_2$. Equivalent matrices may readily be constructed for other values of p and q.

Now the transfer matrix for one complete cycle may be constructed from a product of $2(p + q)$ matrices of these two forms. For the particular case of the Helmholtz motion, the result is

$$\boldsymbol{M} = \boldsymbol{M}_1^{2p} \boldsymbol{M}_2^{2q} \tag{15}$$

since there are $2q$ sticking intervals followed by $2p$ slipping intervals, with the time discretisation in use here. The result $\boldsymbol{M}$ is a real matrix, which will not in general be symmetric. If all the eigenvalues of $\boldsymbol{M}$ lie inside the unit circle in the complex plane, then all possible perturbations must decay and the Helmholtz

motion is stable. At the threshold of stability, the first eigenvalue crosses the unit circle. Its phase will indicate the order of subharmonic associated with the instability pattern. The precise pattern of the most unstable perturbation can be found from the eigenvector(s) (and the associated principal vectors, if there are repeated eigenvalues which do not have distinct eigenvectors) [15].

It is equally easy to write down an equivalent of eq. (15) for any other underlying periodic solution to the Raman model. The rich set of possible solutions, and a procedure for finding them when a piecewise-linear friction curve is assumed, have been described in a companion paper [2]. Given any such solution, one simply constructs the product of matrices $\boldsymbol{M}_1$ and $\boldsymbol{M}_2$ in the order which matches the required pattern of sticking and slipping in one period. If the slipping velocity in the underlying periodic solution varies at different time steps, then for the stability analysis the friction curve must be linearised around these different values in turn. This means that the matrices $\boldsymbol{M}_1$ will not all have the same value of ζ, but this poses no extra difficulty for the computation.

2.4. Results without torsional coupling

We examine first some computed results for the stability of the Helmholtz motion in the absence of torsional interaction. For the example described in the previous section, results for the eigenvalues for the parameter values $\lambda = 0.99$, $\zeta = 0.01$, $\gamma = 1$ are given in Table I. The first column lists the magnitudes of the eigenvalues, which in this case are all less than unity so that the Helmholtz motion is stable for this case. (Note that all values are repeated twice. This is a consequence of the fact that this formulation of the problem uses a state vector of double the size which is strictly necessary, in order to maintain a direct correspondence with the space-time diagram. A modification to the formulation to avoid this inefficiency will be described in section 3.1.) The second column shows the calculated phase of the eigenvector, divided by 2π, and the third column shows the subharmonic order which follows from this phase.

Table I. Results for the Helmholtz solution to Raman's model with $p = 2$, $q = 3$, $\lambda = 0.99$, $\zeta = 0.01$, $\gamma = 1$.

Magnitude of eigenvalue	Phase of eigenvalue ($\div 2\pi$)	Order of subharmonic
0.9801	0	1
0.9801	0	1
0.9866	0.3333	3
0.9866	−0.3333	3
0.9866	0.3333	3
0.9866	−0.3333	3
0.9899	0.5000	2
0.9899	0.5000	2
0.9964	0	1
0.9964	0	1

In this case the eigenvalue closest to the unit circle corresponds to an order-one "unsubharmonic", a perturbation pattern with the same periodicity as the Helmholtz motion itself. (More will be said in the next subsection on the physical interpretation of such "unsubharmonic" perturbation patterns.) A simple iteration based on linear interpolation may now be used to vary ζ and search for the condition at which the most unstable eigenvector crosses the unit circle. The critical value of ζ for this example is found to be 0.0122. Numerical experiments reveal that for general β (without torsional interaction) the threshold depends (to a first approximation) only on the value of $\alpha = \zeta/\varepsilon$, as was found in the case $\beta = 1/n$ analysed in the previous subsection. For the example problem, the stability threshold is thus $\alpha \approx 1.22$.

One interesting fact revealed in Table I seems to apply to the general case, according to extensive numerical experiments. The subharmonic orders associated with the eigenvalues go no higher than the values associated with the elemental subharmonic paths available with the assumed value of β. Since $2 < 1/\beta < 3$, elemental paths give second and third subharmonics, but if the space-time diagram is drawn out in detail for this problem (not reproduced here) it becomes apparent that, with the interaction between elemental paths, one can only guarantee a repeat of the pattern after 2×3 periods. Of course, a general combination of the eigenvalues listed in Table I will produce a pattern which only repeats after six cycles, but it is interesting that the individual eigenvalues never seem to correspond to this long periodicity.

Computed stability thresholds for a wide range of values of p and q, for the Helmholtz motion with no torsional interaction, are plotted in Fig. 7. Specifically, all values $p = 1, \ldots, 10$, $q = p, \ldots, 20$ have been examined. The subharmonic orders associated with the most unstable perturbations are also plotted in Fig. 7, as the dashed line. A reflection coefficient $\lambda = 0.9995$ was chosen for these computations, very close to unity so that the results could be compared with the approximate result (13) for the cases $\beta = 1/n$, as a check. Agreement is obtained within the expected accuracy of that formula. Also, the calculated subharmonic order is found to vary with n in the manner predicted in section 2.2.

In computing these results, the friction curve has been assumed to have a constant slope for all slipping velocities. This is, of course, physically unrealistic, but

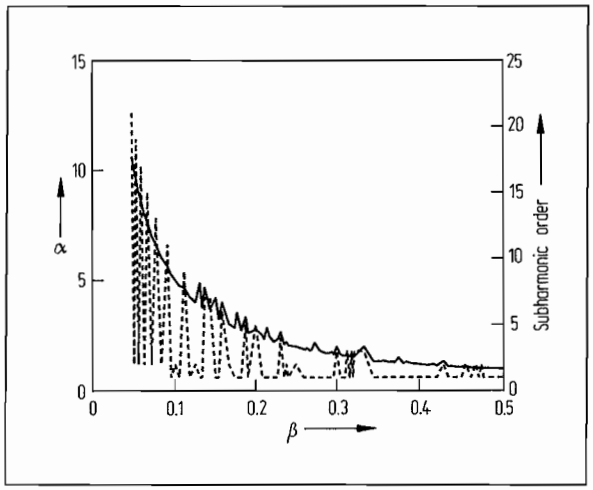

Fig. 7. Solid line: stability threshold α for the Helmholtz solution to the Raman model, plotted against β. Dashed line: the subharmonic order for the least stable eigenvector, which determines the threshold. Results are shown for all cases $p = 1, \ldots, 10$, $q = p, \ldots, 20$.

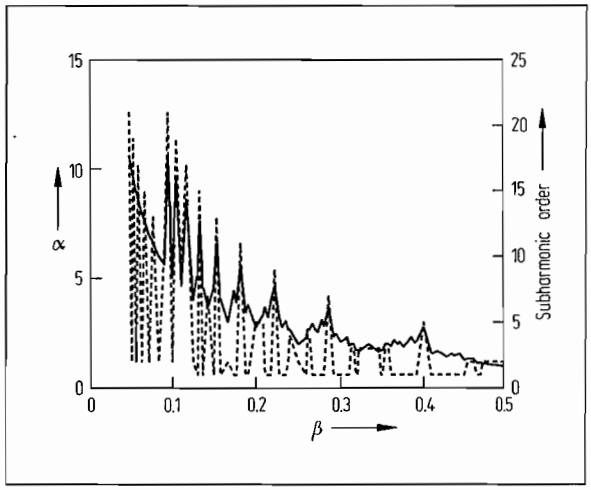

Fig. 8. Stability threshold and subharmonic order in the same format as Fig. 7, for periodic solutions to Raman's model having a slip time equal to half the value for the Helmholtz motion.

it is computationally convenient. It corresponds to the case for which a procedure for calculating a rather general set of periodic solutions has been presented, in the companion paper [2]. Interestingly, the precise form of the periodic solution does not matter when this assumption is made, since variations of slipping velocity do not make any difference to the calculation. The only role of the underlying periodic solution is to define the sequence of sticking and slipping states at the bow-string contact. As was described in section 2.3, there is no difficulty in incorporating the effect of an arbitrary friction curve into the formalism used here. The term M_1^{2p} in eq. (15) would simply be replaced by a product of $2p$ matrices, each having the form of eq. (14) but with varying values of ζ calculated from the slope of the friction curve at the slipping velocity appropriate to the underlying periodic solution at each successive time step.

It is straightforward to apply this procedure to periodic solutions other than the Helmholtz motion. In Fig. 8, results are plotted in the same form as Fig. 7 for the stability threshold and critical subharmonic order, for single-slip-per-cycle solutions in which the slip time is taken to be p time intervals per cycle, rather than $2p$ as in the Helmholtz motion. All that need be changed to make this calculation is that eq. (15) is replaced by

$$M = M_1^p M_2^{2q+p}. \tag{16}$$

To see more clearly what has happened to the stability threshold when the slipping time is thus halved, Fig. 9 shows the ratio of the two cases. The threshold is never decreased, but in some cases it is unchanged.

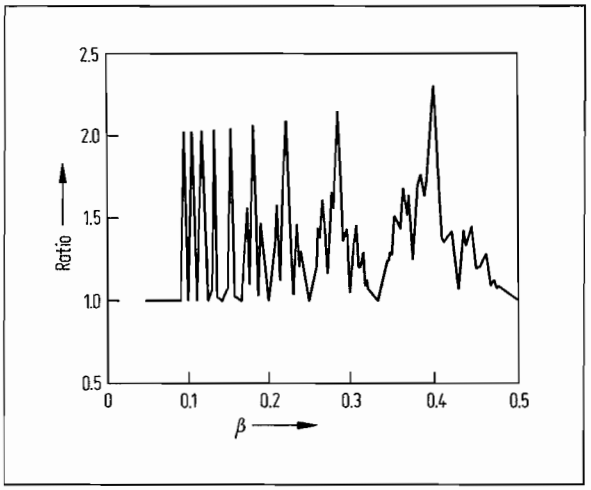

Fig. 9. Ratio of the values of α for the two cases shown in Figs. 8 and 7.

The detailed pattern of change is seen to be rather complicated, ranging up to rather more than a factor of two for certain values of p and q.

It is of some interest to compare the results so far with the most naive estimate of the behaviour of the stability threshold, suggested again by the space-time diagram. The threshold of stability occurs when the effect of amplification at the slipping bow is just balanced by dissipative effects. In the model as it has been studied so far, dissipative effects occur only at the terminations of the string. If all details of subharmonic paths and so on are ignored, a crude estimate of the condition of balance would be given by requiring that

the strength of amplification, multiplied by the fraction of the time in which it can happen, should equal the strength of dissipation, multiplied by its time of availability (which is all the time, at both ends of the string). We might take the strength of amplification to be 2ζ, the total amount "created" in one interaction like Fig. 3b, and the corresponding measure of the strength of dissipation would be ε. The condition then yields

$$2\zeta \times (\text{fractional slipping time}) \approx 2\varepsilon,$$

so that

$$\alpha \approx 1/(\text{fractional slipping time}). \qquad (17)$$

(This is essentially the argument and result discussed by Weinreich and Caussé [14].) For the Helmholtz motion, the fractional slipping time is $\beta = p/(p+q)$, so that (17) is within a factor two of the result (13). This simple prediction also follows the trend of the computed results in Fig. 7. When the slipping time is halved, (17) suggests that the threshold would be doubled. Fig. 9 shows that this is at least of the correct order of magnitude, but that there are quite large variations for different values of β, and in most cases the increase in threshold is rather less than this value. However all the results so far can be thought of as detailed variations superimposed on this simple behaviour, determining by the subtleties of subharmonic paths and their interactions in eigenvector combinations.

The simple argument suggests that no particular regime of periodic oscillation is favoured over another on grounds of stability, except in so far as their fractional slipping times vary. In practice, however, the Helmholtz motion is usually obtained more readily than other oscillation regimes, and one might ask whether stability considerations play any part in this apparent preference. It is therefore natural to enquire whether the detailed computed results reveal anything which goes against the negative conclusion of the simple argument. Fig. 10 shows stability thresholds for a range of values of β and of slipping time (assuming a single slip per cycle). The values of $p:q$ are 3:16, 4:15, 5:14, 6:13 and 7:12 (so that the number of time steps per Helmholtz period is always equal to 38 within the formulation in use here). For each case, slipping is allowed for $1, 2, 3, \ldots, 30$ time steps.

The ideal Helmholtz cases are indicated by circles. The figure shows that the stability threshold increases monotonically as slipping decreases, for any given values of p and q. There are no local maxima, for the Helmholtz motion or for any other slipping time. However, the Helmholtz motion is seen to be special in a certain sense: it lies at the edge of a plateau. There is a sharp drop in the stability threshold for slipping

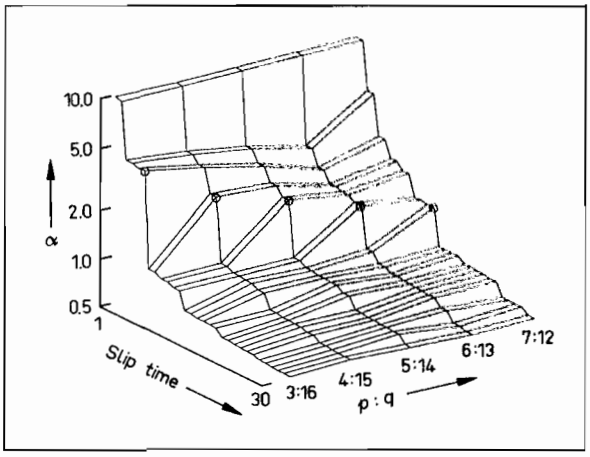

Fig. 10. Variation of stability threshold α in the Raman model, for a range of values of p and q and of slipping time. The threshold is plotted on a logarithmic scale. The ringed points mark the Helmholtz solution for each value of $p:q$.

times longer than the Helmholtz value, and there is no immediate rapid increase for shorter slipping times. This is not sufficient evidence on its own to account for the apparent preference real bowed strings exhibit for the Helmholtz motion, but within the limits of validity of the Raman model it is at least suggestive.

2.5. The influence of torsional coupling

Torsional coupling, modelled in the simple way described in section 2.1, dissipates energy from the transverse waves on the string. It might be expected to have similar effects to boundary dissipation, discussed in sections 2.2–2.4, but as Weinreich and Caussé have pointed out [14] its effects are actually rather more complicated. Boundary dissipation is inescapable: whatever combination of amplitudes on elemental subharmonic paths one chooses, there is always some loss. Torsional coupling, on the other hand, is selective. As will be seen shortly, it is possible for cancellation to occur when the waves incident on the two sides of the sticking bow are equal in amplitude.

It is convenient to start with an example in which there is no boundary damping. Table 2 gives the magnitudes and phases of the eigenvalues of the transfer matrix, for perturbations to an ideal Helmholtz motion with $p = 2$, $q = 5$, $\lambda = 1$, $\zeta = 0.01$ and $\gamma = 0.9$. (Only one of each pair of repeated eigenvalues is listed.) This value of γ represents a quite modest level of coupling to torsion [8], but it is sufficient to produce very large decay rates for almost all perturbation eigenvectors. The exceptions all correspond to "unsubharmonic" patterns, with eigenvalue phases of zero. There are two pairs of these, one being exactly neutrally stable (magnitude unity) and the other being unstable.

The neutrally stable pair of eigenvalues correspond to a perturbation pattern which is easily written down. The form is quite general, not restricted to these particular values of p and q. Consider a pair of vectors

$$\boldsymbol{v}_1 = [v, \eta, -\eta, -v, v, \eta \ldots]^t,$$
$$\boldsymbol{v}_2 = [-\eta, -v, v, \eta, -\eta, -v, v \ldots]^t. \quad (18)$$

It is easily verified that when $\lambda = 1$, for any matrix $\boldsymbol{M}_1$ of the form defined in eq. (14)

$$\boldsymbol{M}_1 \boldsymbol{v}_1 = \boldsymbol{v}_2, \quad \boldsymbol{M}_1 \boldsymbol{v}_2 = \boldsymbol{v}_1. \quad (19)$$

Identical results hold for the transformation matrix during sticking, $\boldsymbol{M}_2$. So any vector of the form $\boldsymbol{v}_1$ is an eigenvector of any matrix formed from an even number of products of matrices $\boldsymbol{M}_1$ and $\boldsymbol{M}_2$, with eigenvalue unity. This it represents a neutrally stable perturbation to any periodic solution whatever to the Friedlander model (i.e. the Raman model with $\lambda = 1$). It is easy to see what this means physically: the vector $\boldsymbol{v}_1$ always presents waves of equal magnitude and opposite sign incident from the two sides of the bow. As Fig. 11 shows, when the interactions of Fig. 3 are thus superimposed, the result is as if the bow had not been there, and the two waves carry on unchanged. This is equally true of slipping or sticking.

The unstable pair of "unsubharmonic" eigenvalues in Table II correspond to what Weinreich and Caussé have called "between-the-raindrops motion" [14]. This also involves cancellation at the bow in the manner shown in Fig. 11, but this time it is selective. The perturbation pattern is such that equal incident waves always arrive at the sticking bow, so that there is no loss into torsional waves, but the incident waves at the slipping bow are not equal, and so there is some amplification. The result is a pattern which is unstable in the presence of arbitrarily strong dissipation into torsional waves at the sticking bow. It requires some boundary dissipation to stabilise it, in the manner discussed in previous subsections.

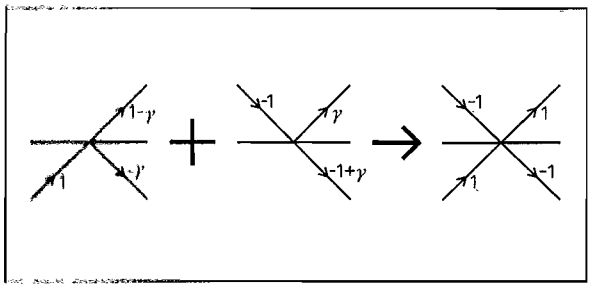

Fig. 11. Cancellation of the effects of torsional coupling at the sticking bow when the incident perturbation amplitudes from the two sides have equal amplitude but opposite sign. A similar picture applies to the slipping bow under the same circumstances.

Table II. Results for the Helmholtz solution to Raman's model with $p = 2$, $q = 5$, $\lambda = 1$, $\zeta = 0.01$, $\gamma = 0.9$. Only one of each pair of repeated eigenvalues is shown.

Magnitude of eigenvalue	Phase of eigenvalue ($\div 2\pi$)
0.8040	0.5000
0.8040	0.2479
0.8040	−0.2479
0.8053	0.3321
0.8053	−0.3321
1.0000	0
1.0116	0

It is important to note that "between-the-raindrops motion" is not possible for $\beta = 1/n$. The Raman model gives a constraint on the average velocity at the bowed point, which can only differ very slightly from zero (for values of λ close to unity). The underlying periodic solution will satisfy this constraint, so any perturbation pattern must give an average velocity at the bowed point of zero. For "between-the-raindrops motion" the perturbation at the bow is only non-zero during slipping, so there must be at least two different values of velocity at the bowed point during an episode of slipping, at least one of which must be positive and one negative (unless the perturbation velocity at the bow is identically zero at all times, which is the uninteresting case discussed above, neutrally stable when $\lambda = 1$). For $\beta = 1/n$, the Raman model allows only one value of velocity during slipping, and so there can be no "between-the-raindrops" pattern. This argument is confirmed by the analysis in section 2.2: only one eigenvalue with zero phase was found when $\beta = 1/n$, and that was shown to correspond to the uninteresting case with no amplification at the slipping bow. An example of a growing instability with a "between-the-raindrops" pattern for $\beta \neq 1/n$ will be shown shortly.

More detail of the behaviour of the eigenvalues in the presence of torsional coupling may be revealed by a root-locus plot. Fig. 12 shows the paths in the complex plane of all eigenvalues, as γ is decreased from unity to 0.6, all other parameters being the same as for the example in Table II. Initially, all eigenvalues are on or just outside the unit circle, since there is no dissipative mechanism operating. Their positions around the unit circle show the expected mixture of first, second, third and fourth subharmonics, since $1/4 < p/(p+q) < 1/3$. As γ decreases, all eigenvalues except those with zero phase move rapidly inwards as they are damped by torsional coupling. Once the loss rate per cycle ceases to be a small quantity, the phases cease to correspond accurately to subharmonics. The

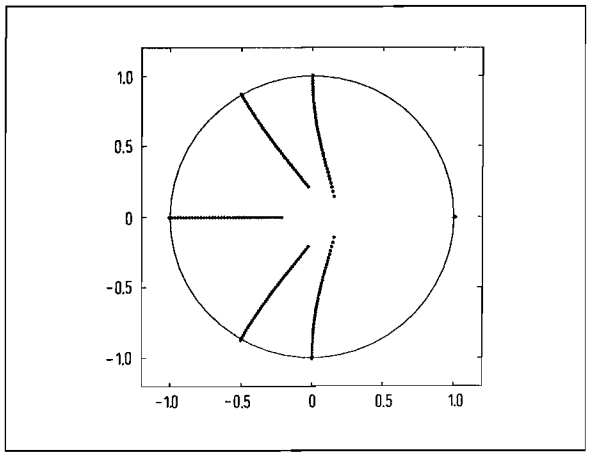

Fig. 12. Root-locus plot in the complex plane, for the eigenvalues of the stability analysis for the Helmholtz solution to Raman's model with $p = 2$, $q = 5$, $\lambda = 1$ and $\zeta = 0.01$, as γ varies from unity to 0.6. The unit circle is shown.

eigenvalues with zero phase are unaffected by the value of γ, as just described.

Computations can be made of the stability threshold for a range of values of β, in much the same way as described in section 2.4. Results are shown in Fig. 13, for $\gamma = 0.9$. The qualitative features are just as would be expected from the discussion above. For $\beta \neq 1/n$, the threshold is governed by the least stable "between-the-raindrops" perturbation pattern. The value of the threshold is governed by a balance between amplification at the slipping bow and boundary dissipation, just as in the cases without torsional coupling. As before, it depends only on the ratio $\alpha = \zeta/\varepsilon$. The order of magnitude is much as before, and for some values of p and q the value is exactly the same since the same perturbation pattern is responsible.

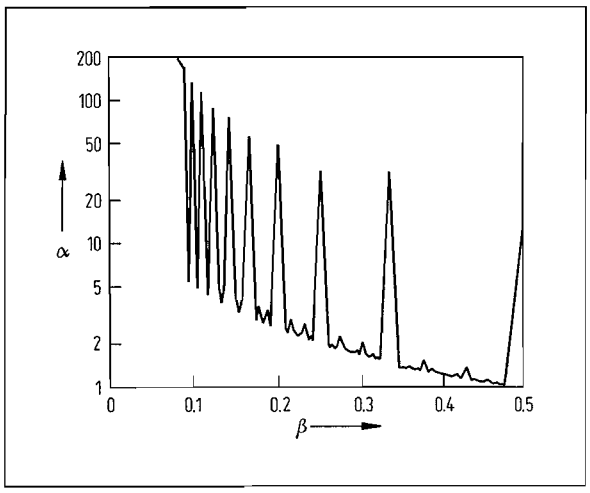

Fig. 13. Stability threshold α for the Helmholtz solution to the Raman model with $\gamma = 0.9$, plotted against β in the same format as Figs. 7 and 8, except that the vertical scale is logarithmic here to accommodate the large range of values.

At the points $\beta = 1/n$, things are very different. To calculate the threshold value, amplification at the slipping bow is increased until an eigenvalue crosses the unit circle, but now this has to be one of the eigenvalues strongly affected by dissipation from torsional coupling. Very large amplification is thus needed, and the stability threshold is very high. The parameter α is no longer really appropriate to characterise it, since it is governed by the balance of amplification and torsional loss, boundary dissipation being a small perturbation. For the purpose of Fig. 13, α is nevertheless used, for comparability of the rest of the figure with Figs. 7 and 8. In practice, the very high thresholds of stability at the points $\beta = 1/n$ mean that stability is simply not an issue there. Other factors influencing the maximum and minimum bow force at and near those points are far more important [2], and if the Helmholtz motion is possible at one of these points, it will be stable in the presence of any appreciable torsional dissipation.

Finally, it is interesting to compare these results for the stability of periodic solutions of Raman's model with the results of time-marching transient simulation. The natural parameter to vary in such a simulation in order to explore thresholds of stability is the bow force f_b. We take the case $p = 2$, $q = 5$, $Y_0 = 2$, $\lambda = 0.99$ and $\gamma = 0.9$. A linear friction curve during slipping is assumed, so that ζ is directly proportional to bow force, with no dependence on the value of slipping velocity. The limit of sticking friction is assumed to be $0.8 f_b$, and the friction/velocity relation during slipping is taken to be

$$f(v) = f_b[0.3 + 0.01\, v]. \tag{20}$$

The threshold of stability for the Helmholtz motion is then found to be $f_b = 1.75$, using the analysis method described above.

For $\beta \neq 1/n$, as in this example, we might guess that the unstable growth of a "between-the-raindrops" pattern superimposed on an initial Helmholtz motion will eventually terminate when the negative velocity perturbation becomes large enough to cause sticking when slipping had been assumed. The Helmholtz motion might then give way to a periodic regime with a shorter slipping interval (whose stability could in turn be investigated). This sequence of events is precisely what does occur in the simulation. This is illustrated in Fig. 14, which shows several two-period "snapshots" from a long simulation. The simulation is initialised with a Helmholtz motion with a very small level of superimposed perturbation, as shown in Fig. 14a. The bow force is given the value 2.0, a little above the stability threshold.

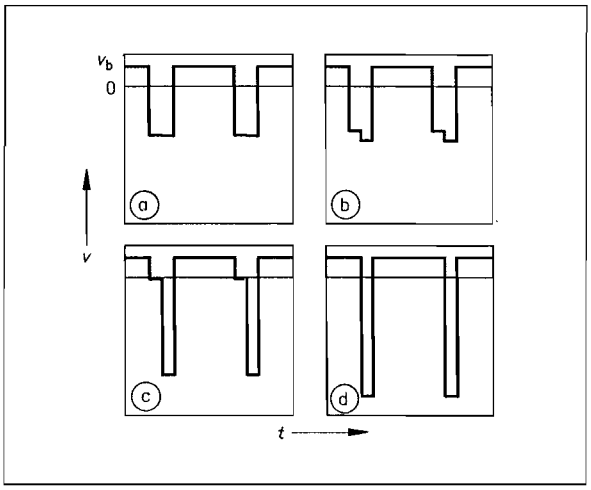

Fig. 14. Four stages in a transient simulation of Raman's model with $p = 2$, $q = 5$, $Y_0 = 2$, $\lambda = 0.99$ and $\gamma = 0.9$, and a bow force $f_b = 2.0$, compared with a stability threshold of 1.75. a) Approximate Helmholtz motion; b) growth of "between-the-raindrops" perturbation; c) growth of the perturbation to large amplitude; d) stable periodic motion with slipping for only one time step per period. Scales are the same in all four cases.

After a few hundred period-lengths, the Helmholtz motion has evolved into the form shown in Fig. 14b. The two values of velocity during slipping are moving apart, one increasing while the other decreases, in the expected pattern for "between-the-raindrops" motion as described above. The growth continues to large amplitudes, as shown in Fig. 14c, and shortly after this stage the string ceases to slip in the first of the two nominal slipping intervals of the original Helmholtz motion. The velocity waveform now settles down to a stable periodic solution with just one interval of slipping per cycle, shown in Fig. 14d. When the stability threshold is calculated for this final motion, it is found to require bow force greater than 77.2, which is above the Schelleng maximum bow force for this problem [4, 7] and so is irrelevant. This large value arises because "between-the-raindrops" perturbations are not possible now there is only one slipping interval per cycle, as explained above.

3. Stability of solutions to rounded-corner models

3.1. Reformulation of the transformation matrices

The Raman model is very convenient for analytic investigation because of its simplicity, but it certainly does not describe the behaviour of real bowed strings very accurately [2]. A significant gain in realism is made when the "rounded-corner model" is used in its place. Here, the delta-function reflections of the Raman model are replaced by convolution with a pair of reflection functions, which represent the combined effects of propagation and boundary reflection [6, 8]. A wide range of different physical models can be included under this heading, by changing the details of these reflection functions.

It would obviously be desirable to be able to analyse stability of periodic solutions to these models. This can be done by a similar approach to that employed for Raman's model, but the formulation of the state vector and its transformation matrices must be changed. The immediate link between elements of the state vector and variation with position along the string is lost, but the new formulation is not only more general, but also more compact. When applied to the Raman model it yields a state vector, and corresponding matrices, with dimension $(p + q)$ rather than $2(p + q)$, which has obvious advantages in computational efficiency.

The entries in the new state vector are simply the past history of the outgoing waves from the bowed point in the two directions. There must be enough of these to allow for the delay on the journeys to the respective ends of the string and back, plus enough extra history to allow the convolution integrals to be carried out (in discrete form) with the desired reflection functions. We may write this vector $[\ldots L_3^{(n)}, L_2^{(n)}, L_1^{(n)}, R_1^{(n)}, R_2^{(n)}, R_3^{(n)}, \ldots]^t$ at the nth time step, where the entries describe outgoing perturbation velocity amplitudes to the left and right of the bowed point with the obvious convention. (This is a different naming convention from the earlier approach, based on the space-time diagram, where the positional coordinate along the string ran vertically, and directions were thought of as "up" and "down". It corresponds to the usage in other accounts of rounded-corner models.)

The transformation matrix for a single time step now has to represent two things. All entries in the state vector except $L_1^{(n)}$ and $R_1^{(n)}$ simply propagate outwards by one place: the matrix entries represent two delay lines. The entries $L_1^{(n)}$ and $R_1^{(n)}$ are calculated by combining two effects. First, the incoming waves from the left and right sides of the bow are calculated by (discrete) convolution over the stored values. Second, these are combined to calculate the new outgoing waves according to the interactions shown in Fig. 3, exactly as in the earlier formulation. Again, different matrices are needed depending on whether the time step in question corresponds to sticking or slipping at the bowed point, but they have very similar forms. To illustrate, consider first the example used in eq. (14) to illustrate the earlier approach: the Raman model with $p = 2$, $q = 3$. When the bow-string contact is slipping,

the transformation is

$$\begin{bmatrix} L_2^{(n+1)} \\ L_1^{(n+1)} \\ R_1^{(n+1)} \\ R_2^{(n+1)} \\ R_3^{(n+1)} \end{bmatrix} = \begin{bmatrix} 0 & 1 & 0 & 0 & 0 \\ -\lambda\zeta & 0 & 0 & 0 & -\lambda(1+\zeta) \\ -\lambda(1+\zeta) & 0 & 0 & 0 & -\lambda\zeta \\ 0 & 0 & 1 & 0 & 0 \\ 0 & 0 & 0 & 1 & 0 \end{bmatrix} \begin{bmatrix} L_2^{(n)} \\ L_1^{(n)} \\ R_1^{(n)} \\ R_2^{(n)} \\ R_3^{(n)} \end{bmatrix} \tag{21}$$

while the corresponding transformation during sticking has ζ replaced by $-\gamma$ in the matrix, just as before. The "convolutions" in this case each consist of single terms, the four terms containing the factor λ. With extended reflection functions, there would be non-zero entries in terms neighbouring these four (involving the discretised values of the reflection function), and it would be necessary to have more of the history stored in the state vector. The unity entries would then extend to the new limits of the matrix along the subdiagonal (in the lower portion of the matrix) and superdiagonal (in the upper portion), to simulate the delay lines for this extra stored history.

3.2. Results with narrow reflection functions

A thorough study of the stability of periodic solutions to rounded-corner models would be a major undertaking, and lies beyond the scope of this article. For the present, just one illustration of the application of the approach will be given. The natural first step away from the Raman model is to consider reflection functions which are of non-zero width, but still narrow compared with the period of the motion [6, 7]. It has been shown that the kernel function necessary to calculate periodic solutions does not then depend (to a first approximation) upon the details of the reflection function, but only on a measure of its width [2]. So we will choose a very simple test case, in which the two reflection functions are identical (apart from their different time delays), time-symmetrical, and with only three non-zero values at the level of discretisation being employed. For the case corresponding to eq. (21), the transformation matrix equation during slipping is then

$$\begin{bmatrix} L_3^{(n+1)} \\ L_2^{(n+1)} \\ L_1^{(n+1)} \\ R_1^{(n+1)} \\ R_2^{(n+1)} \\ R_3^{(n+1)} \\ R_4^{(n+1)} \end{bmatrix} = \begin{bmatrix} 0 & 1 & 0 & 0 & 0 & 0 & 0 \\ 0 & 0 & 1 & 0 & 0 & 0 & 0 \\ -\sigma\zeta & -\lambda\zeta & -\sigma\zeta & 0 & -\sigma(1+\zeta) & -\lambda(1+\zeta) & -\sigma(1+\zeta) \\ -\sigma(1+\zeta) & -\lambda(1+\zeta) & -\sigma(1+\zeta) & 0 & -\sigma\zeta & -\lambda\zeta & -\sigma\zeta \\ 0 & 0 & 0 & 1 & 0 & 0 & 0 \\ 0 & 0 & 0 & 0 & 1 & 0 & 0 \\ 0 & 0 & 0 & 0 & 0 & 1 & 0 \end{bmatrix} \begin{bmatrix} L_3^{(n)} \\ L_2^{(n)} \\ L_1^{(n)} \\ R_1^{(n)} \\ R_2^{(n)} \\ R_3^{(n)} \\ R_4^{(n)} \end{bmatrix} \tag{22}$$

where $[\sigma, \lambda, \sigma]$ are the sampled values of the reflection functions. There is a corresponding matrix during sticking, as in previous cases. For a model which satisfies the physical constraint that the string eventually returns to its undisturbed position following any transient excitation, the values of the reflection function will satisfy

$$\lambda + 2\sigma = 1 . \tag{23}$$

As in previous sections, we first illustrate the results of this procedure by showing the full set of eigenvalues for a specific example. A case has been chosen which is fairly similar to that shown in Table II and Fig. 12. Larger values of p and q are needed now, to provide sufficient resolution in time to allow a reasonably realistic width of reflection functions to be represented. The chosen case has $p = 6$, $q = 16$ and $\zeta = 0.01$, and the reflection functions satisfy eq. (23) with the value $\sigma = 0.05$. Slip time is assumed to be equal to p. The magnitudes and phases of all 24 eigenvalues (corresponding to the dimension of the state vectors) are listed in the first two columns of Table III, when torsional coupling is not included (i.e. $\gamma = 1$).

The results show some features which are by now familiar from the earlier investigation. The phases of the eigenvalues all correspond quite closely to subharmonics, with orders one, two and three. Among the eigenvalues with zero phase, corresponding to "unsubharmonics", there is one which is unstable for this combination of parameters, corresponding to Weinreich and Caussé's "between-the-raindrops" motion, as before [14]. A feature of these results which differs from those of Raman's model is that already, even with no torsional dissipation, many of the eigenvalues have magnitudes well below unity. There are even some with magnitude zero, but these probably arise as an artefact of the particular formulation of state vector in use here and do not seem to be of great interest.

The influence of torsional coupling is examined next. Fig. 15 shows a root locus plot for the example just studied, showing the paths of all eigenvalues in the complex plane as γ is decreased from unity to 0.6 in 20 steps. The full set of eigenvalues in the final state, with $\gamma = 0.6$, is listed in the third and fourth columns

Table III. Results for a rounded-corner model with $\sigma = 0.05$, $\lambda = 0.90$, $p = 6$, $q = 16$, slip time per cycle equal to p, and $\zeta = 0.01$, for two values of γ.

$\gamma = 1$		$\gamma = 0.6$	
Magnitude of eigenvector	Phase of eigenvector ($\div 2\pi$)	Magnitude of eigenvector	Phase of eigenvector ($\div 2\pi$)
1.001	0	1.002	0
0.968	0.334	0.965	0
0.968	−0.334	0.912	0
0.964	0	0.890	0
0.911	0	0.872	0
0.910	0.500	0.785	0
0.890	0	0.743	0
0.871	0	0.729	0
0.871	0.334	0.702	0
0.871	−0.334	0.678	0
0.781	0	0.640	0
0.758	0.334	0.193	0.266
0.758	−0.334	0.193	0.266
0.743	0	0.183	0.500
0.728	0	0.174	0.266
0.727	0.500	0.174	0.266
0.701	0	0.151	0.266
0.679	0	0.151	−0.266
0.675	0.334	0.146	0.500
0.675	−0.334	0.135	0.266
0.640	0	0.135	−0.266
0.000	0	0.000	0
0.000	0.500	0.000	0
0.000	0.500	0.000	0.500

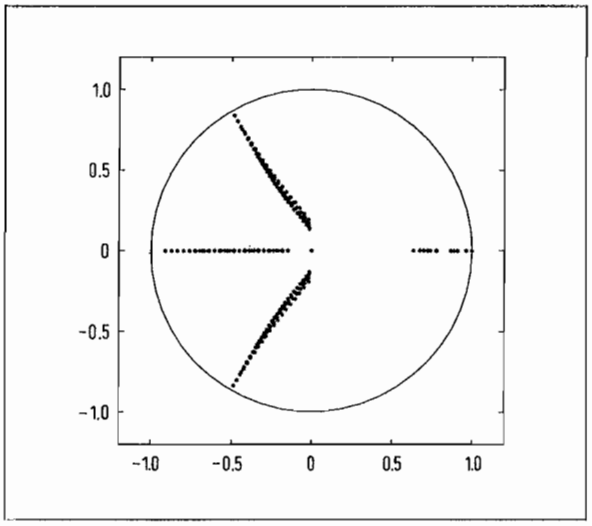

Fig. 15. Root-locus plot in the complex plane for the 24 eigenvalues of the stability analysis of a periodic solution to the simple rounded-corner model described in the text, having $p = 6$, $q = 16$ and $\zeta = 0.01$, reflection functions which satisfy eq. (23) with the value $\sigma = 0.05$, and a slip time equal to p, showing results as γ is decreased from unity to 0.6 in 20 steps. The unit circle is also shown.

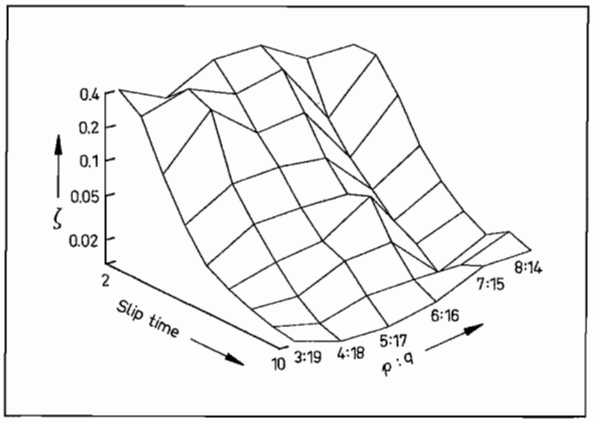

Fig. 16. Variation of stability threshold ζ in the rounded-corner model described in the text, for a range of values of p and q and of slipping time. The threshold is plotted on a logarithmic scale.

of Table III. The general pattern is similar to that seen earlier for Raman's model, although the details are of course different. All eigenvalues with non-zero phases are heavily damped by the torsional coupling, but the ones with zero phase are virtually unaffected. One remains unstable, and even appears to have become slightly more unstable, although this may be an artefact of computational inaccuracy.

Next, we examine the variation with p, q and slip time. Results have been computed for cases with $p:q = 3:19$, $4:18$, $5:17$, $6:16$, $7:15$ and $8:14$ – it is necessary to keep $p + q$ constant, so that the width of the reflection functions remains the same for comparability. The value $\sigma = 0.05$ is again used to specify this width. In each case, the slipping time was allowed to range from 2 to 10 time steps per period. (Note that slipping time plays a rather different role in rounded-corner models from that in the Raman model: the slipping time of the Helmholtz motion now depends on the width of the reflection functions and the value of the bow force, and must be established in any particular case by careful solution of the periodic motion problem [2].) It is sufficient for this preliminary investigation to show only results without torsional coupling.

Fig. 16 shows a plot of the threshold value of ζ for instability, in the same format as Fig. 10, which shows a corresponding result for the Raman model (although with somewhat different parameter values). The patterns revealed by the two figures are quite different. With reflection functions of finite width, there is no obvious sign of a "cliff edge" marking the slip time of the Helmholtz motion for the various values of $p:q$, which was the most conspicuous feature of Fig. 10. Fig. 16 is in fact rather featureless. The

Table IV. Ratio of stability thresholds for two different rounded-corner models, for a range of values of p, q and slip time per cycle. The numerator model has $\sigma = 0.05$ and $\lambda = 0.90$, the denominator model has $\sigma = 0.02$ and $\lambda = 0.96$.

Slip time	$p:q$					
	3:19	4:18	5:17	6:16	7:15	8:14
2	1.867	2.842	2.614	3.132	2.347	2.861
3	2.721	3.119	2.057	3.074	2.368	2.935
4	2.687	2.874	2.282	2.236	2.414	2.500
5	2.593	2.718	2.583	2.459	2.451	2.402
6	2.588	2.616	2.563	2.617	2.386	2.465
7	2.563	2.579	2.584	2.663	2.523	2.541
8	2.550	2.557	2.586	2.595	2.547	2.561
9	2.546	2.548	2.560	2.586	2.556	2.576
10	2.539	2.537	2.545	2.549	2.591	2.589

threshold value, on this logarithmic scale, decays rather smoothly with slip time, interrupted ocasionally by small increases.

Finally, this calculation has been repeated with reflection functions which are narrower, with $\sigma = 0.02$. The ratios of the stability thresholds for the two models are listed in Table IV. It is very suggestive that in most cases the value is close to 2.5, the ratio of the two reflection function widths. Any detailed interpretation of these results would need to be made in the context of the discussion in the companion paper [2] of the variation with slip time of the underlying periodic solution to this rounded-corner model. Such detailed interpretations would require a more lengthy discussion than is appropriate in this study, and the issue will not be pursued further here.

4. Conclusions

Methods have been presented for analysing the stability of periodic solutions to Raman's model and the rounded-corner models of bowed-string motion. These have been illustrated with representative examples, and the physical mechanisms responsible for stabilising and destabilising the various possible periodic solutions have been investigated. In the case of Raman's model, a fairly complete picture may have been established, although there are certainly opportunities for further study. In the case of the rounded-corner models, only a very preliminary account has been given, and much might be learned from a more thorough investigation.

One particular avenue which might yield interesting results would involve combining this analysis of stability with the systematic simulations described elsewhere [7]. These have employed large-scale parallel computation to explore the regions of parameter space within which the Helmholtz motion arises from a given initial transient. It would be possible to take the end state of such a set of simulations, and for each point for which a periodic solution has been achieved, to carry through a stability analysis using the particular form of that periodic solution. That would lead to a parameter-space map of the degree of stability of the Helmholtz motion, and the other periodic solutions encountered. It might shed further light on the relative robustness of the different oscillation regimes within a given model, and on the variations of this pattern between models.

Acknowledgement

The author is very grateful to Dr. Michael McIntyre and Professor Bob Schumacher for their invaluable contributions during the many years that this work has taken to reach fruition.

References

[1] Raman, C. V., On the mechanical theory of vibrations of bowed strings. Indian Assoc. Cult. Sci. Bull. **15** [1918], 1–158.
[2] Woodhouse, J., Idealised models of a bowed string. Acustica **79** [1993], 233–250.
[3] McIntyre, M. E., Woodhouse, J., A parametric study of the bowed string: the violinist's menagerie. J. Catgut Acoust. Soc. **42** [1984], 18–21.
[4] Schelleng, J. C., The bowed string and the player. J. Acoust. Soc. Amer. **53** [1973], 26–41.
[5] Cremer, L., The physics of the violin. MIT Press, Cambridge MA, USA 1985.
[6] Woodhouse, J., On the playability of violins, Part 1, Reflection functions. Acustica **78** [1993], 125–136.
[7] Woodhouse, J., On the playability of violins, Part 2, Minimum bow force and transients. Acustica **78** [1993], 137–153.
[8] McIntyre, M. E., Schumacher, R. T., Woodhouse, J., On the oscillations of musical instruments. J. Acoust. Soc. Amer. **74** [1983], 1325–1345.
[9] Woodhouse, J., Physical modelling of bowed strings. Computer Music J. (in press).
[10] McIntyre, M. E. Woodhouse, J., On the fundamentals of bowed-string dynamics. Acustica **43** [1979], 93–108.
[11] McIntyre, M. E., Schumacher, R. T., Woodhouse, J., Aperiodicity in bowed-string motion. Acustica **49** [1981], 13–32; see also Acustica **50** [1982], 294–295.
[12] Schelleng, J. C., The violin as a circuit. J. Acoust. Soc. Amer. **35** [1963], 326–338.
[13] Friedlander, F. G., On the oscillations of a bowed string. Proc. Cambridge Philos. Soc. **49** [1953], 516–530.
[14] Weinreich, G., Caussé, R., Elementary stability considerations for bowed-string motion. J. Acoust. Soc. Amer. **89** [1991], 887–895.
[15] See for example Gantmacher, F. R., The theory of matrices. (English translation by K. A. Hirsch.) Chelsea publishing company, New York 1977 (Volume 1), 1960 (Volume 2).